

## APPLICATION OF THE METHODS OF NUMERICAL MODELING TO EVALUATION OF THE TOTAL-PRESSURE LOSS IN GAS TURBINES

K. N. Volkov

UDC 532.529:536.24

*The total-pressure loss in gas turbines is evaluated. Reynolds-averaged Navier–Stokes equations are used for numerical calculations. The Spalart–Allmaras model, the  $k$ – $\epsilon$  model, and the two-layer model and their different modifications allowing for the rotation of the flow and the curvature of streamlines are used to close these equations. The role of different corrections to the turbulence models for the accuracy of calculated estimates is elucidated.*

**Introduction.** When modern gas-turbine engines are created, it is impossible, in practice, to avoid using numerical methods of calculation of the internal turbulent flows and heat exchange of a viscous compressible gas in regions of complex geometric configuration.

Calculation of flows in gas-turbine engines involves the modeling of turbulent heat exchange under the influence of favorable and unfavorable pressure gradients, free convection, flows with allowance for the rotation and swirl of the flow, surface roughness, the interaction of vortex structures with the surface, etc. [1, 2]. The trend shown by the gas temperature at the inlet of the blade passage toward increasing to  $T = 1800$ – $2000$  K makes it necessary to ensure the appropriate cooling of the surfaces in flow (the injection of a cold gas into the boundary layer and film cooling are, particularly, used).

One basic factor exerting an influence on the efficiency of combustion of fuel is the total-pressure loss. The loss in gas turbines is due to the formation of boundary layers on the walls, the occurrence of shock-wave structures for large Mach numbers, the mixing of flows behind turbine blades, and to secondary flows and is dependent on many factors, in particular on the parameters of the flow at the channel inlet, the turbine-blade angle, and the airfoil shape. Experimental investigations [3, 4] have made it possible to elucidate the mechanisms of loss and to reveal the role of individual factors.

Theoretical computation of the energy loss caused by the flow passing through the grid is usually reduced to determination of the potential pressure distribution along the blade contour, calculation of the laminar and turbulent boundary layers on the airfoil, and computation of the energy loss by mixing in cocurrent flow behind the grid. The state of the art in methods of computational gas dynamics enables one to evaluate the loss in gas turbines on the basis of a complex approach. In computational investigations, the standard  $k$ – $\epsilon$  turbulence model and the method of wall functions are mainly used, which makes it impossible to obtain accurate and reliable estimates of the total-pressure loss [5, 6].

In this work, on the basis of the results of numerical modeling of turbulent flows of a viscous compressible gas, we evaluate the total-pressure loss for two configurations of a blade passage (low- and high-pressure turbines) and draw conclusions on their correctness. To close Reynolds equations we use different turbulence models (Spalart–Allmaras model, the  $k$ – $\epsilon$  model, and the two-layer model) and elucidate the role of different corrections for the accuracy of calculations. To numerically solve the problem we use the condition of spacing of flow.

**Basic Equations.** In the Cartesian coordinate system  $(x, y, z)$ , nonstationary flow of a compressible gas is described by the equation

$$\frac{\partial Q}{\partial t} + \frac{\partial F_x}{\partial x} + \frac{\partial F_y}{\partial y} + \frac{\partial F_z}{\partial z} = 0,$$

which is supplemented with the gas equation

$$p = (\gamma - 1) \rho \left[ e - \frac{1}{2} (v_x^2 + v_y^2 + v_z^2) \right].$$

Here

$$\mathbf{Q} = \begin{pmatrix} \rho \\ \rho v_x \\ \rho v_y \\ \rho v_z \\ \rho e \end{pmatrix}; \quad \mathbf{F}_x = \begin{pmatrix} \rho v_x \\ \rho v_x v_x + p - \tau_{xx} \\ \rho v_x v_y - \tau_{xy} \\ \rho v_x v_z - \tau_{xz} \\ (\rho e + p) v_x - v_x \tau_{xx} - v_y \tau_{xy} - v_z \tau_{xz} + h_x \end{pmatrix};$$

$$\mathbf{F}_y = \begin{pmatrix} \rho v_y \\ \rho v_y v_x - \tau_{yx} \\ \rho v_y v_y + p - \tau_{yy} \\ \rho v_y v_z - \tau_{yz} \\ (\rho e + p) v_y - v_x \tau_{yx} - v_y \tau_{yy} - v_z \tau_{yz} + h_y \end{pmatrix}; \quad \mathbf{F}_z = \begin{pmatrix} \rho v_z \\ \rho v_z v_x - \tau_{zx} \\ \rho v_z v_y - \tau_{zy} \\ \rho v_z v_z + p - \tau_{zz} \\ (\rho e + p) v_z - v_x \tau_{zx} - v_y \tau_{zy} - v_z \tau_{zz} + h_z \end{pmatrix}.$$

The components of the viscous-stress tensor and the components of the heat-flux vector are found from the relations

$$\tau_{ij} = \mu_{\text{ef}} \left( \frac{\partial v_i}{\partial x_j} + \frac{\partial v_j}{\partial x_i} - \frac{2}{3} \frac{\partial v_k}{\partial x_k} \delta_{ij} \right), \quad h_i = -\lambda_{\text{ef}} \frac{\partial T}{\partial x_i}.$$

The effective viscosity and thermal conductivity represent the sum of molecular and turbulent transfer coefficients

$$\mu_{\text{ef}} = \mu + \mu_t, \quad \lambda_{\text{ef}} = c_p \left( \frac{\mu}{\text{Pr}} + \frac{\mu_t}{\text{Pr}_t} \right).$$

To obtain the value of molecular viscosity as a function of temperature we use the Sutherland law

$$\frac{\mu}{\mu_*} = \left( \frac{T}{T_*} \right)^{3/2} \frac{T_* + B}{T + B},$$

where  $\mu_* = 1.68 \cdot 10^{-1}$  kg/(m·sec),  $T_* = 273$  K, and  $B = 110.5$  K for air. The molecular thermal conductivity is related to the Prandtl number. The molecular and turbulent Prandtl numbers are assigned constant values ( $\text{Pr} = 0.72$  and  $\text{Pr}_t = 0.9$  for air).

**Turbulence Models.** For calculation of the turbulent viscosity (or related quantities) we use different turbulence models.

*Standard k-ε model.* The equations of the turbulence model are written in the Launder–Spalding formulation [7] with a Kato–Launder correction for the term of turbulence production [8] and a correction for the curvature of streamlines [9, 10].

In the model [7], the turbulence-generation term is found from the relation

$$P = \mu_t |S|^2, \quad |S| = (2S_{ij}S_{ij})^{1/2}.$$

To allow for the rotation of the flow, we modify it as follows [8]:

$$P = \mu_t |S| |\Omega|, \quad |\Omega| = (2\Omega_{ij}\Omega_{ij})^{1/2}.$$

The components of the strain-rate tensor and the vorticity are computed from the formulas

$$S_{ij} = \frac{1}{2} \left( \frac{\partial v_i}{\partial x_j} + \frac{\partial v_j}{\partial x_i} \right), \quad \Omega_{ij} = \frac{1}{2} \left( \frac{\partial v_i}{\partial x_j} - \frac{\partial v_j}{\partial x_i} \right).$$

Summation over double subscripts is assumed.

To allow for the curvature of streamlines we introduce, into the formula for calculation of the turbulent viscosity, the damping function [9]

$$\mu_t = c_\mu \rho \frac{k^2}{\varepsilon} f(\text{Ri}_t), \quad f(\text{Ri}_t) = \frac{1}{1 + c \text{Ri}_t}.$$

For calculation of the turbulent Richardson number we use the formula [10]

$$\text{Ri}_t = \left( \frac{k}{\varepsilon} \right)^2 \left[ \frac{q}{R} (\mathbf{b} \cdot \boldsymbol{\omega}) \right].$$

The local radius of curvature is found from the relation

$$R = \frac{1}{|\ddot{\mathbf{r}}|} = \left[ \left( \frac{\partial^2 x}{\partial s^2} \right)^2 + \left( \frac{\partial^2 y}{\partial s^2} \right)^2 + \left( \frac{\partial^2 z}{\partial s^2} \right)^2 \right]^{-1/2}.$$

By  $s$  we mean the coordinate reckoned along the streamline ( $q = ds/dt$ ). The tangent, the normal, and the binormal to the streamline are found from the Frenet triangle formulas:

$$\boldsymbol{\tau} = \frac{\mathbf{q}}{q}, \quad \mathbf{n} = \frac{\ddot{\mathbf{r}}}{|\ddot{\mathbf{r}}|} = R \ddot{\mathbf{r}}, \quad \mathbf{b} = \boldsymbol{\tau} \times \mathbf{n} = \frac{R}{q} \mathbf{q} \times \ddot{\mathbf{r}}.$$

As a result, the formula for calculation of the Richardson number takes the form [10]

$$\text{Ri}_t = \left( \frac{k}{\varepsilon} \right)^2 (\mathbf{q} \times \ddot{\mathbf{r}}) \cdot \boldsymbol{\omega}.$$

*Two-layer model.* In the model [11], the wall region is subdivided into two subregions the boundary between which is dependent on the local Reynolds number  $\text{Re}_y = \rho k^{1/2} y / \mu$ . The standard  $k$ - $\varepsilon$  model [7] is used for  $\text{Re}_y > \text{Re}_{y^*}$ , whereas the one-parameter  $k$ - $l$  turbulence model [12] is used for  $\text{Re}_y < \text{Re}_{y^*}$ . We take  $\text{Re}_{y^*} = 180$ .

*Spalart–Allmaras model.* In the model [13], the vorticity

$$H = |\boldsymbol{\Omega}|$$

is used for calculation of the source term related to the generation of turbulent viscosity. Also, the modified form of representation of the source term

$$H = |\boldsymbol{\Omega}| + 2 \min \{ 0, |S| - |\boldsymbol{\Omega}| \}$$

is used.

**Boundary Conditions on the Wall.** To obtain the parameters of the flow near the wall we use the method of wall functions [7] (for the  $k$ - $\varepsilon$  model) and [14] (for the Spalart–Allmaras model). The condition  $\partial k / \partial n = 0$  is set on the wall in the case where the two-layer model is used. No boundary condition on the wall is required for the dissipative function.

For the method of wall functions to be realized, it is necessary that  $y^+ \gg 1$ . The use of the two-layer model requires that  $y^+ \sim 1$ , where  $y^+ = yu_\tau/\nu$ ,  $u_\tau = (\tau_w/\rho)^{1/2}$ .

**Total-Pressure Loss.** In the one-dimensional case the total-pressure-loss factor is computed from the formula

$$L = \frac{p_{01} - p_{02}}{\rho_1 u_1^2 / 2}$$

or

$$L = \frac{p_{01} - p_{02}}{p_{01} - p_1}$$

The above relations give identical values for incompressible flow. The difference between them increases with Mach number at entry into the computational domain (it amounts to 4% for  $M = 0.4$ ). For incompressible flow, we easily obtain the relationship between the total-pressure-loss factor and the pressure coefficient

$$L = 1 - \left( \frac{A_1}{A_2} \right)^2 - C_p.$$

The pressure coefficient is expressed by the difference of static pressures and the velocity head:

$$C_p = \frac{p_2 - p_1}{\rho_1 u_1^2 / 2}.$$

To calculate the total-pressure loss in the three-dimensional case we use the same relations but expressed by the averaged quantities [2]. In particular, one widely uses the following determination:

$$L = \frac{p_{01} - p_{02}}{p_{01}},$$

where

$$p_{01} = \frac{1}{A_1} \oint_{A_1} p_0 dA; \quad p_{02} = \frac{1}{A_2} \oint_{A_2} p_0 dA.$$

**Numerical Method.** Discretization of the Navier–Stokes equations and the equations of the turbulence model is carried out on an unstructured grid using the control-volume method [15]. A five-step Runge–Kutta method is used for discretization of time derivatives. Convective terms are discretized on the basis of the MUSCL scheme of 2nd order written with the use of the diagram of normalized variables [16] (the minmod flow limiter is used). Centered difference formulas of 2nd order are used for discretization of diffusion flows.

The system of difference equations is solved by the multigrid method on the basis of the total-approximation scheme (four grid levels and a V cycle are used).

**Calculation Results.** We consider two different configurations of the computational domain which correspond to low- and high-pressure turbines.

*Low-pressure turbine.* The geometry of the blade passage of a low-pressure turbine is shown in Fig. 1a. Gas enters the computational domain through the boundary ABCD at which we prescribe the flow velocity in parallel to the upper and low boundaries ( $q = 38.80$  m/sec), the total-pressure profile  $p_0 = p_0(z)$  shown in Fig. 1b ( $p_{0m} = 4.27 \cdot 10^4$  Pa), the stagnation temperature ( $T_0 = 298$  K), and the characteristics of turbulence. The latter include the value of the modified turbulent viscosity for the Spalart–Allmaras model ( $\tilde{\nu}_0 = 10^{-4}$  m<sup>2</sup>/sec) and the values of the kinetic turbulence energy and the rate of its dissipation for the  $k$ – $\epsilon$  model ( $k_0 = 10^{-4}$  m<sup>2</sup>/sec<sup>2</sup> and  $\epsilon_0 = 10^{-3}$  m<sup>2</sup>/sec<sup>3</sup>).

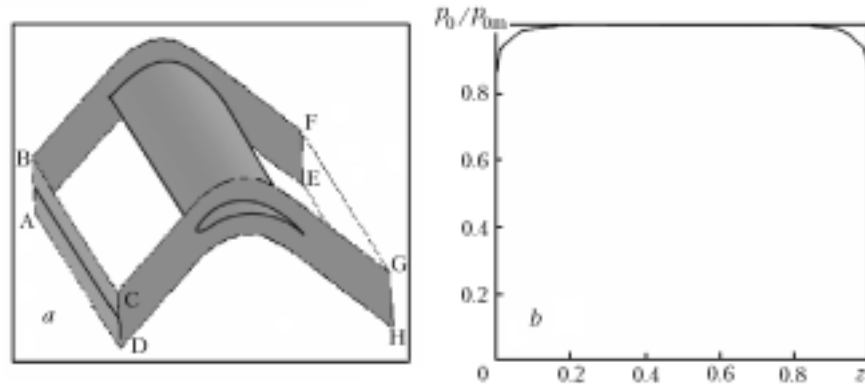


Fig. 1. Blade passage of a low-pressure turbine: the geometry of the computational domain (a) and the total-pressure profile in the inlet cross section (b).

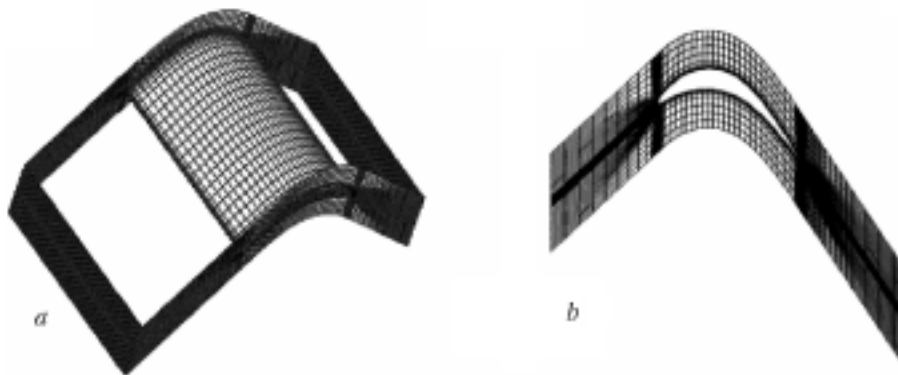


Fig. 2. Computational grid (a) and the grid in the middle cross section (b).

TABLE 1. Total-Pressure-Loss Factor (Low-Pressure Turbine)

Model	$L$ , %
Experiment [17]	2.1205
Spalart–Allmaras model	2.1225
$k$ – $\epsilon$ model with a Kato–Launder correction	2.0335
$k$ – $\epsilon$ model with a correction for streamline curvature	2.1186
Two-layer model	2.0681

The static pressure ( $p = 3.08 \cdot 10^4$  Pa) is prescribed at the outlet boundary EFGH. At the boundaries ABFE and DCGH and on the airfoil surface, we set the boundary sticking and nonflow conditions for the tangential and normal velocity components and the wall temperature ( $T_w = 300$  K). Periodic boundary conditions are used at the boundaries BFGC and AEHD.

The calculations are carried out on an unstructured grid containing 105,066 nodes and 95,760 cells (Fig. 2). The inlet and outlet boundaries contain 1368 cells, whereas the periodic boundaries contain 3268 cells; the wall includes 8992 cells.

The total-pressure distributions in the middle cross section of the outlet boundary and the total-pressure-loss factor as a function of the number of iterations, which have been obtained on the basis of different turbulence models, are shown in Fig. 3. The standard Spalart–Allmaras model and its modified version enable us to reach the prescribed level of discrepancy after 94 and 96 iterations. When the standard  $k$ – $\epsilon$  model is used, the convergence is incomplete (the discrepancy exceeds the prescribed value after 1000 multigrid cycles); the introduction of a correction for streamline curvature gives convergence after 164 iterations.

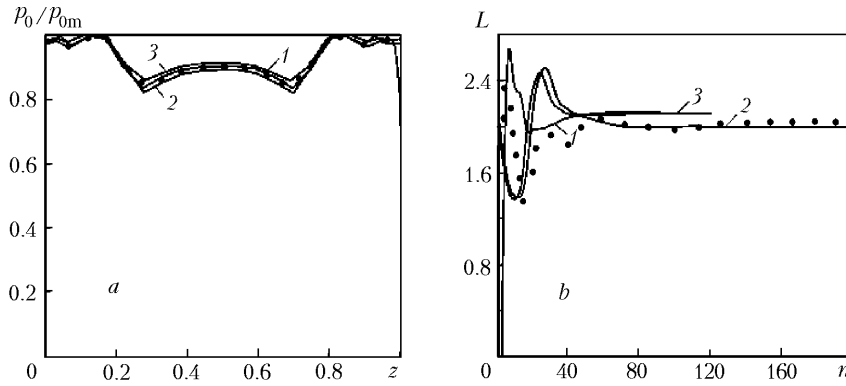


Fig. 3. Total-pressure loss in the outlet cross section (a) and the change in the total-pressure-loss factor as a function of the number of iterations (b): 1) Spalart-Allmaras model; 2)  $k-\epsilon$  model; 3)  $k-\epsilon$  model with a correction for streamline curvature; points, two-layer model.

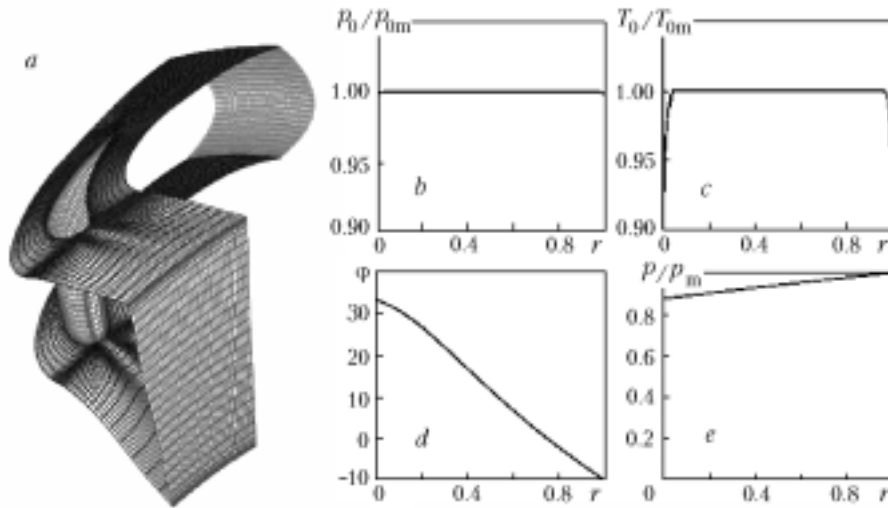


Fig. 4. Blade passage of a high-pressure turbine: the geometry of the computational domain (a), the radial profiles of the total pressure (b), the stagnation temperature (c), and the angle prescribing the flow direction (d) in the inlet cross section and the radial profile of the static pressure in the outlet cross section (e).

Data on the total-pressure loss are summarized in Table 1 and are compared to the results of measurements [17]. The difference in the results obtained on the basis of the Spalart-Allmaras models and different versions of the  $k-\epsilon$  model amounts to nearly 2%. The error obtained on the basis of the turbulence model is attributed to the insufficient grid resolution in the boundary layer.

*High-pressure turbine.* The geometry of the blade passage of a high-pressure turbine is shown in Fig. 4a. In the inlet cross section of the computational domain, we prescribe the radial profiles of the total pressure  $p_0 = p_0(r)$  ( $p_{0m} = 3.44 \cdot 10^5$  Pa), the stagnation temperature  $T_0 = T_0(r)$  ( $T_{0m} = 373$  K), and the angle showing the flow direction  $\varphi_0 = \varphi_0(r)$  (Fig. 4b, c, and d) and the value of the modified turbulent viscosity for the Spalart-Allmaras model ( $\tilde{\nu}_0 = 8.8 \cdot 10^{-5}$  m<sup>2</sup>/sec) or the value of the kinetic turbulence energy and the rate of its dissipation for the  $k-\epsilon$  model ( $k_0 = 10^{-4}$  m<sup>2</sup>/sec<sup>2</sup> and  $\epsilon_0 = 10^{-3}$  m<sup>2</sup>/sec<sup>3</sup>). The radial static-pressure profile  $p = p(r)$  ( $p_m = 2.2 \cdot 10^5$  Pa) is used in the outlet cross section; no other boundary conditions are required here (Fig. 4d).

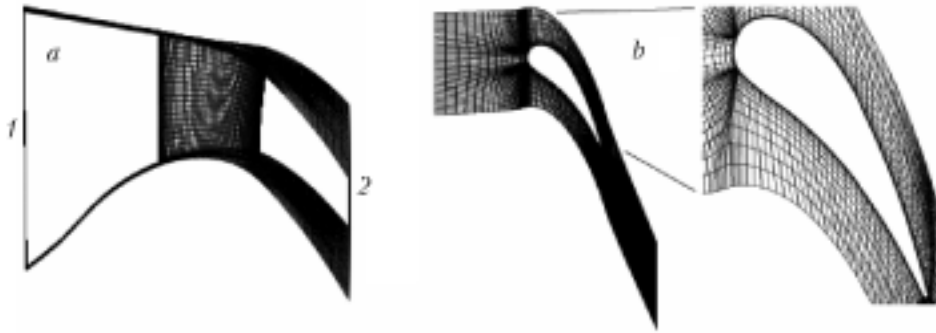


Fig. 5. Computational grid (a) (1) inlet boundary and 2) outlet boundary) and the grid in the middle cross section (b).

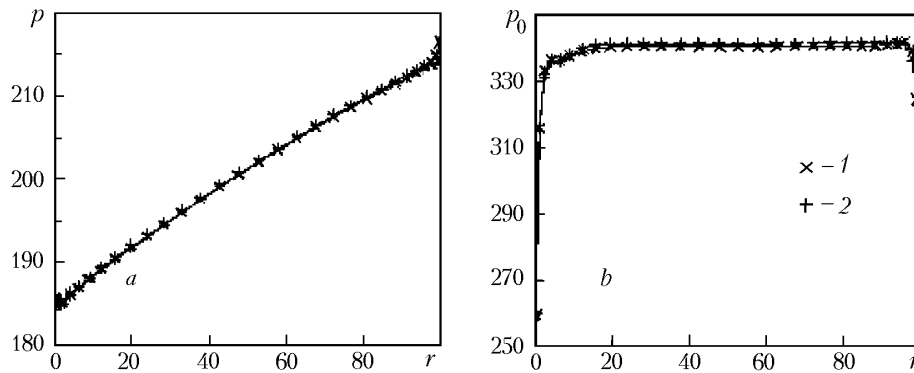


Fig. 6. Radial distributions of the static (a) and total (b) pressures in the outlet cross section: 1) Spalart–Allmaras model; 2)  $k-\epsilon$  model.

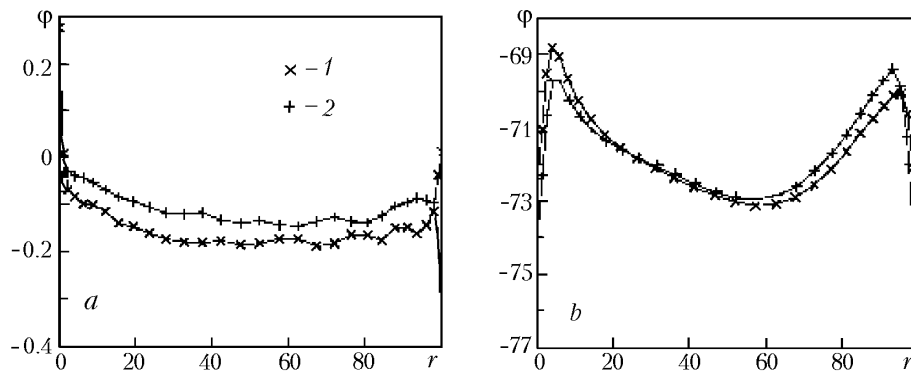


Fig. 7. Radial distributions of the swirl angle in the inlet (a) and outlet (b) cross sections: 1) Spalart–Allmaras model; 2)  $k-\epsilon$  model.

Boundary sticking and nonflow conditions for the tangential and normal velocity components and the wall temperature ( $T_w = 298$  K) are set on the walls and the surface of the turbine blade. Periodic boundary conditions are used at the left and right boundaries.

Calculations are carried out on a hybrid grid (Fig. 5) containing 123,765 nodes and 113,328 cells of which 20,480 cells are arranged at the boundary. The structured part of the grid near the airfoil has dimensions  $95 \times 41 \times 37$ . The inlet boundary contains 4001 cells, the outlet boundary contains 5001 cells, the periodic boundaries contain 3384 cells, the lower and upper walls contain 3148 cells, and the airfoil surface contains 4336 cells.

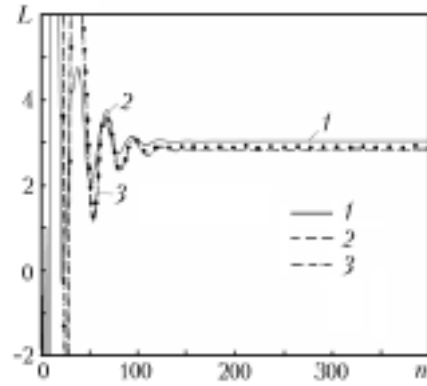


Fig. 8. Change in the total-pressure-loss factor as a function of the number of iterations: 1) Spalart-Allmaras model; 2)  $k$ - $\epsilon$  model with a Kato-Lauder correction; 3)  $k$ - $\epsilon$  model without a Kato-Lauder correction, points,  $k$ - $\epsilon$  model with a correction for streamline curvature.

TABLE 2. Total-Pressure-Loss Factor (High-Pressure Turbine)

Model	$L, \%$	
	$n = 400$	$n = 1000$
<i>Experiment [17]</i>	3.1002	3.1002
Spalart-Allmaras model	3.1416	3.1416
Modified Spalart-Allmaras model	3.1153	3.1153
$k$ - $\epsilon$ model with a Kato-Lauder correction	2.8212	2.8166
$k$ - $\epsilon$ model without a Kato-Lauder correction	2.8489	2.8304
$k$ - $\epsilon$ model with a correction for streamline curvature	2.8294	2.8405

The distributions of the flow characteristics sought are shown in Figs. 6 and 7. Whereas the turbulence models give nearly identical distributions of total pressure in the outlet cross section (Fig. 6b), the distributions of the swirl angle of the flow differ (Fig. 7b) mainly near the walls of the blade passage.

The total-pressure-loss factor as a function of the number of iterations is plotted in Fig. 8. The difference between the results obtained on the basis of the Spalart-Allmaras model and the  $k$ - $\epsilon$  model amounts to about 10%.

Data on the total-pressure loss are summarized in Table 2 and are compared to measurement results [17]. The introduction of Kato-Lauder corrections and a correction for the curvature of streamlines improves the calculated estimates of the total pressure, obtained on the basis of the  $k$ - $\epsilon$  turbulence model.

**Conclusions.** On the basis of the results of numerical modeling of the turbulent flows of a viscous compressible gas, we have evaluated the total-pressure loss for two configurations of the blade passage (low- and high-pressure turbines) and have drawn conclusions on their correctness. It has been shown that the introduction of corrections for the curvature of streamlines and for rotation improves the properties of the  $k$ - $\epsilon$  model and the Spalart-Allmaras model. The results obtained can be used for improving the efficiency of gas-turbine plants, whereas the numerical method developed can be applied to their optimization.

## NOTATION

$A$ , cross-sectional area,  $m^2$ ;  $\mathbf{b}$ , binormal vector;  $B$ , constant in the Sutherland law,  $K$ ;  $c$ , constant;  $c_p$ , specific heat at constant pressure,  $J/(kg \cdot K)$ ;  $c_\mu$ , constant in the turbulence model;  $C_p$ , pressure coefficient;  $e$ , total energy of a unit mass,  $J/kg$ ;  $f$ , damping function;  $\mathbf{F}$ , flow vector;  $h$ , heat-flux density,  $W/m^2$ ;  $H$ , source term;  $k$ , kinetic turbulence energy,  $m^2/sec^2$ ;  $l$ , linear scale,  $m$ ;  $L$ , total-pressure-loss factor,  $\%$ ;  $n$ , number of iterations;  $\mathbf{n}$ , normal vector;  $M$ , Mach number;  $p$ , pressure,  $Pa$ ;  $P$ , term of turbulence generation,  $m^2/sec^3$ ;  $Pr$ , Prandtl number;  $q$ , velocity value,  $m/sec$ ;  $\mathbf{q}$ ,



velocity vector, m/sec;  $\mathbf{Q}$ , vector of conservative variables;  $r$ , radial coordinate, m;  $\mathbf{r}$ , radius vector, m;  $R$ , radius of curvature, m;  $Re$ , Reynolds number;  $Ri$ , Richardson number;  $s$ , coordinate reckoned along the streamline, m;  $S$ , strain-rate tensor;  $t$ , time, sec;  $T$ , temperature, K;  $u$ , average velocity, m/sec;  $u_\tau$ , dynamic velocity, m/sec;  $v_x$ ,  $v_y$ , and  $v_z$ , velocity components, m/sec;  $x$ ,  $y$ ,  $z$ , Cartesian coordinates, m;  $\gamma$ , ratio of specific heats;  $\delta_{ij}$ , Kronecker symbol;  $\epsilon$ , rate of dissipation of turbulent energy  $m^2/sec^3$ ;  $\lambda$ , thermal conductivity, W/(m·K);  $\mu$ , dynamic viscosity, kg/(m·sec);  $\nu$ , kinematic viscosity,  $m^2/sec$ ;  $\rho$ , density,  $kg/m^3$ ;  $\tau$ , tangential stress, N/m;  $\boldsymbol{\tau}$ , tangential vector;  $\phi$ , angle prescribing the flow direction, deg;  $\omega$ , vortex;  $\Omega$ , vorticity. Subscripts and superscripts: ef, effective parameters of a turbulent flow;  $i$ ,  $j$ , and  $k$ , tensor indices; m, maximum; t, parameters of a turbulent flow;  $x$ ,  $y$ , and  $z$ , projections on the coordinate axis; w, wall;  $\tau$ , shear stress; 0, stagnation parameters; 1 and 2, inlet and outlet cross sections; \*, critical parameters; +, dimensionless parameters in the boundary layer;  $\cdot$ , time derivative;  $\sim$ , modified turbulent viscosity.

## REFERENCES

1. V. K. Garg, Heat transfer research on gas turbine aerofoil at NASA GRC, *Int. J. Heat Fluid Flow*, **23**, 109–136 (2002).
2. A. Klein, Characteristics of combustor diffusers, *Progr. Aerospace Sci.*, **31**, 171–271 (1995).
3. S. J. Payne, R. W. Ainsworth, R. J. Miller, R. W. Moss, and N. W. Harvey, Unsteady loss in a high pressure turbine stage, *Int. J. Heat Fluid Flow*, **24**, 698–708 (2003).
4. L. Helmers, R. Johnsson, and S. Trollheden, Modelling turbine performance at large tip clearance of unshrouded rotor cascades, *AIAA Paper*, No. 2003–4767 (2003).
5. P. Koutmosa and J. J. McGuirk, CFD predictions of lobed mixer performance, *Comput. Meth. Appl. Mech. Eng.*, **122**, 131–144 (1995).
6. A. D. Walker, P. A. Denman, and J. J. McGuirk, Experimental and computational study of hybrid diffusers for gas turbine combustors, *J. Eng. Gas Turbines Power*, **126**, 717–725 (2004).
7. B. E. Launder and D. B. Spalding, The numerical computation of turbulent flows, *Comput. Meth. Appl. Mech. Eng.*, **3**, 269–289 (1974).
8. M. Kato and B. E. Launder, The modelling of turbulent flow around stationary and vibrating square cylinders, in: *Proc. 9th Symp. on Turbulent Shear Flows*, 16–18 August 1993, Kyoto, Japan (1993), Vol. 9, pp. 10.4.1–10.4.6.
9. M. A. Leschziner and W. Rodi, Calculation of annular and twin parallel jets using various discretization schemes and turbulent model variations, *ASME J. Fluid Eng.*, **103**, 353–360 (1981).
10. I. A. Belov and S. A. Isaev, *Modeling of Turbulent Flows* [in Russian], Izd. BG TU, St. Petersburg (2001).
11. W. Rodi, Experience with two-layer models combining the  $k$ - $\epsilon$ -model with one-equation model near wall, *AIAA Paper*, No. 91–0216 (1991).
12. M. Wolfshtein, The velocity and temperature distribution of one-dimensional flow with turbulence augmentation and pressure gradient, *Int. J. Heat Mass Transfer*, **12**, 301–318 (1969).
13. P. R. Spalart and S. R. Allmaras, A one-equation turbulence model for aerodynamic flows, *AIAA Paper*, No. 92–0439 (1992).
14. S. Deck, P. Duveau, P. d’Espiney, and P. Guillen, Development and application of Spalart–Allmaras one-equation turbulence model to three-dimensional supersonic complex configurations, *Aerospace Sci. Technol.*, **6**, 171–183 (2002).
15. K. N. Volkov, Application of the control-volume method to solving the problems of fluid mechanics on unstructured grids, *Vychisl. Metody Programmir.*, **6**, No. 1, 43–60 (2005).
16. K. N. Volkov, Discretization of convective flows in the Navier–Stokes equations on the basis of high-resolution difference schemes, *Vychisl. Metody Programmir.*, **5**, No. 1, 129–145 (2004).
17. N. W. Harvey, Heat transfer studies of an HP NGV in annular cascade in the pyestock ILPC, *Rolls-Royce Report*, No. B2D2–96D, TRE 90191 (1992).